Ligand Field Splitting on the Xe 4d Core Levels in XeF_x (x = 2, 4, 6) Compounds from High-Resolution Gas-Phase Photoelectron Spectra: The Structure of XeF_6

J. N. Cutler,[†] G. M. Bancroft,*[,†] J. D. Bozek,[†] K. H. Tan,[†] and G. J. Schrobilgen[‡]

Contribution from the Department of Chemistry and Centre for Chemical Physics, University of Western Ontario, London, Ontario, Canada N6A 5B7, Canadian Synchrotron Radiation Facility, Synchrotron Radiation Centre, University of Wisconsin, Stoughton, Wisconsin 53589, and Department of Chemistry, McMaster University, Hamilton, Ontario, Canada L8S 4M1.
Received May 16, 1991

Abstract: Using monochromatized synchrotron radiation, high-resolution (total line widths of ~ 0.2 eV) Xe 4d photoelectron spectra are reported for the three xenon fluorides, XeF_x (x = 2, 4, 6). The splitting of the Xe $4d_{3/2}$ and $4d_{5/2}$ core levels is due to the ligand field splitting on the Xe 4d ion state. The splitting is due to the asymmetric C_2^0 crystal field term, which transforms like the electric field gradient as normally measured by Mössbauer spectroscopy or NQR. The appreciable ligand field splitting in XeF_6 shows immediately that XeF_6 is considerably distorted from octahedral symmetry. We have derived the bond angles for the C_{3v} XeF_6 structure using the C_2^0 for XeF_6 and an additive treatment which has been shown to work well for e^2qQ values, giving estimates of $\Theta_{1,2,3} = 50 \pm 2°$ and $\Theta_{4,5,6} = 76 \pm 4°$. These values are in good agreement with the latest theoretical determinations for these angles.

Introduction

Since the discovery of the first noble-gas compounds in 1962,[1] the xenon fluorides (XeF_2, XeF_4, and XeF_6) have been of great chemical interest. The geometric and electronic structures of XeF_2 and XeF_4 have been investigated by different spectroscopic[1-4] and theoretical techniques.[1,5-10] A model based on a three-center four-electron bond, similar to that applied to CO_2, has been used to explain the bonding in the hypervalent structures of XeF_2 ($D_{\infty h}$, linear) and XeF_4 (D_{4h}, square planar).[11,12]

Although the structures and bonding for XeF_2 and XeF_4 have been widely accepted for many years, the structure of XeF_6 *in the gas phase* has remained a puzzle for theoreticians and experimentalists to this day. (The complex solid-state structure has been determined:[13] a cubic unit cell contains 24 tetramers and 9 hexamers of XeF_6 in which XeF_5^+ units are bound through fluorine bridges.) According to the three-center four-electron model, gas-phase XeF_6 should have an octahedral structure. On the other hand, simple valence-shell electron repulsion rules (VSEPR)[14,15] predict that XeF_6 should be a monocapped octahedron with a sterically active lone pair of electrons.

Early electron diffraction work on XeF_6 by Gavin and Bartell[16] and Pitzer and Bernstein[17] was explained by a single C_{3v} configuration with large nonbonded vibrational amplitudes which distorted the molecule from an octahedral structure along a soft t_{1u} bending mode. This structure was supported by infrared and Raman studies of Claassen et al.[18] who reported many more vibrational frequencies than should be expected of an O_h molecule vibrating harmonically.

Later electric field deflection results[19] showed a substantially smaller dipole moment (≈0 D) than should be observed in the structure determined by Gavin and Bartell.[16] This was explained by a second-order Jahn-Teller pseudorotation along a large amplitude T_{1u} bending mode which was coupled with the T_{2g} bending mode.

Several theoretical calculations have been undertaken in an attempt to clarify the structure of XeF_6. Rothman et al.[20] did a pseudopotential SCF-MO study which showed that XeF_6 was distorted from O_h symmetry along the t_{1u} bending mode, to give a C_{3v} structure with the long bonds adjacent to the lone pair. This calculation supported the VSPER model and showed that the molecule existed in a single ground-state configuration with unusual physical properties. A more recent calculation by Klobukowski et al.[21] reported that XeF_6 had two local minima which were stabilized by 20 kcal mol^{-1} when the symmetry of the molecule was lowered from O_h to C_{3v} and C_{2v}.

Experimental and theoretical work has proven that XeF_6 is a nonrigid molecule with local minima giving C_{3v} and C_{2v} geometries via a pseudorotation mechanism.[22,23] The determination of the exact structures at each of these minima are currently unresolved and can only be determined by techniques which are fast compared to the fluxionality of the molecule. The time scale of photoelectron

* Author to whom correspondence should be addressed.
[†] University of Western Ontario and University of Wisconsin.
[‡] McMaster University.

(1) (a) *Noble Gas Compounds*, Hyman, H. H., Ed.; University of Chicago Press: Chicago, IL, 1963; and references therein. (b) Bartlett, N.; Slodky, F. O. *Comprehensive Inorganic Chemistry*; Pergaman Press: Oxford, 1973; Chapter 6.
(2) (a) Agron, P. A.; Begun, G. M.; Levy, H. A.; Mason, A. A.; Jones, C. G.; Smith, D. F. *Science* **1963**, *139*, 842-843. (b) Reichmann, S.; Schreiner, F. *J. Chem. Phys.* **1969**, *51*, 2355-2358.
(3) (a) Siegel, S.; Gebert, E. *J. Am. Chem. Soc.* **1963**, *85*, 240. (b) Templeton, D. H.; Zalkin, A.; Forester, J. D.; Williamson, S. M. *J. Am. Chem. Soc.* **1963**, *85*, 242.
(4) Levy, H. A.; Agron, P. A. *J. Am. Chem. Soc.* **1963**, *85*, 241-242.
(5) Lohr, L. L., Jr.; Lipscomb, W. N. *J. Am. Chem. Soc.* **1963**, *85*, 240-241.
(6) Coulson, C. A. *J. Chem. Soc.* **1964**, 1442-1454.
(7) Basch, H.; Moskowitz, J. W.; Hollister, C.; Hankin, D. *J. Chem. Phys.* **1971**, *55*, 1922-1933.
(8) Carroll, T. X.; Shaw, R. W., Jr.; Thomas, T. D.; Kindle, C.; Bartlett, N. *J. Am. Chem. Soc.* **1974**, *96*, 1989-1996.
(9) Bartell, L. S.; Rothman, M. J.; Ewig, C. S.; Van Wazer, J. R. *J. Chem. Phys.* **1980**, *73*, 367-374.
(10) Herndon, W. C. *J. Mol. Struct. (Theochem)* **1988**, *169*, 389-401, and references therein.
(11) Lombardi, E.; Ritter, R.; Jansen, L. *Int. J. Quantum Chem.* **1973**, *7*, 155-171.
(12) Lombardi, E.; Pirola, L.; Tarantini, G.; Jansen, L.; Ritter, R. *Int. J. Quantum Chem.* **1974**, *8*, 335-345.
(13) Burbank, R. D.; Jones, G. R. *J. Am. Chem. Soc.* **1974**, *96*, 43-48.
(14) Gillespie, R. J.; Nyholm, R. S. *Q. Rev. Chem. Soc.* **1957**, *11*, 339-380.
(15) Gillespie, R. J.; Hargitti, I. *The VSEPR Model of Molecular Geometry*; Allyn and Bacon: Boston, MA, 1991.
(16) Gavin, R. M., Jr.; Bartell, L. S. *J. Chem. Phys.* **1968**, *48*, 2460-2465. Bartell, L. S.; Gavin, R. M., Jr. *J. Chem. Phys.* **1968**, *48*, 2466-2483.
(17) Pitzer, K. S.; Bernstein, L. S. *J. Chem. Phys.* **1975**, *63*, 3849-3856.
(18) Claassen, H. H.; Goodman, G. L.; Kim, H. *J. Chem. Phys.* **1972**, *56*, 5042-5053.
(19) Bernstein, L. S.; Pitzer, K. S. *J. Chem. Phys.* **1975**, *62*, 2530-2534.
(20) Rothman, M. J.; Bartell, L. S.; Ewig, C. S.; Van Wazer, J. R. *J. Chem. Phys.* **1980**, *73*, 375-381.
(21) Klobukowski, M.; Huzinaga, S.; Seijo, L.; Barandiarán, Z. *Theor. Chim. Acta* **1987**, *71*, 237-245.
(22) Strauss, H. L. *Ann. Rev. Phys. Chem.* **1983**, *34*, 301-328.
(23) Christe, K. O.; Wilson, W. W. *Inorg. Chem.* **1989**, *28*, 3275-3277.

0002-7863/91/1513-9125$02.50/0

spectroscopy ($<10^{-15}$ s) is several orders of magnitude faster than the rate of pseudorotation in XeF_6 making it an excellent potential tool for the study of the structure. Indeed, the distorted C_{3v} ground state was recently supported by an analysis of the very broad (2.63 eV line width) F1s core level photoelectron spectrum of XeF_6.[24,25] This line width was initially attributed solely to vibrational broadening in an octahedral structure,[25] but Gustev and Boldyrev[24] showed that this broad line could be explained qualitatively by the presence of two chemically shifted F1s peaks of width ~1.8 eV due to two inequivalent fluorines in C_{3v} symmetry.

We felt that a photoelectron study of the ligand field splittings on the Xe 4d level could give more quantitative information on the XeF_6 structure, if high-resolution spectra (total width < 0.2 eV) could be obtained. Indeed, we have already used high-resolution HeI and HeII photoelectron spectroscopy of low-lying (binding energy < 30 eV) core d levels, to characterize bonding and structure in gas-phase compounds of *main-group* elements such as Zn, Cd, Ga, and In.[26-32] The observed ligand field splittings in the core d^9 ion states are analogous to the much better known splittings of valence d levels in transition-metal compounds.[33-35] The splitting is characterized using the usual crystal field and spin-orbit Hamiltonian[32] and results in five peaks. The core level splittings are dominated by the asymmetric component of the crystal field, C_2^0 (or D_5),[32-34] which is proportional to the electric field gradient, eq_n, at the nucleus measured by Mössbauer spectroscopy, NQR, and perturbed angular correlation.[32,36] As with valence level ligand field splittings and nuclear field gradients, the core level C_2^0 values have been shown to be sensitive to the metal, the bonding properties of the ligand, and the structure of the compound.[32]

Additive models, such as the partial quadrupole splitting model,[36] have been successfully applied to determine structure from quadrupole splittings: for example, to distinguish four-, five-, and six-coordinate organometallic Sn compounds and obtain C–Sn–C bond angles.[37] In addition, this model gave ^{129}Xe quadrupole splittings for solid XeF_6 which are consistent with the solid-state structure.[13,38] Because C_2^0 and eq_n are proportional, such additive models should be very useful for obtaining the structure of XeF_6 from Xe 4d ligand field splittings.

There have been three previous attempts to measure Xe 4d splittings in the xenon fluorides,[39-41] including XeF_6.[39] Comes et al.[40] were partially successful in observing the Xe 4d ligand field splittings in XeF_2 and XeF_4 from a detailed high-resolution gas-phase photoabsorption study of the 4d → 6p, 7p transitions. For example, four of the expected five 4d → 6p peaks were resolved for XeF_2; but only two peaks were resolved in the very weak XeF_4 4d → 6p spectrum. These transitions were not even observed for XeF_6,[20] and no estimate of C_2^0 could be made. However, Comes et al. observed the broad $4d^{10}5s^2 \rightarrow 4d^9 5s^2$ "5p" transition and stated that the absorption bands behaved exactly like a molecule of O_h or near O_h symmetry. Such photoabsorption spectra cannot be generally used to obtain core level ligand field splittings because the core → Rydberg transitions are usually very weak and strongly overlap. In a previous photoelectron study[41] of the Xe 3d and 4d levels of XeF_2 and XeF_4, at an instrumental resolution of ~0.6 eV, no ligand field splittings of the $d_{5/2}$ and $d_{3/2}$ levels were observed. However, these lines were broadened relative to Xe gas. This broadening, when deconvoluted with a Gauss–Lorentz function, allowed for a determination of C_2^0. The C_2^0 values from this study were in good agreement with those obtained from the earlier photoabsorption study[40] and consistent with the calculations of Basch[7] on XeF_2 and XeF_4.

It was evident from the above photoabsorption and photoelectron studies that high intensity, high energy (≥100 eV), high resolution (~0.1 eV) photon sources, and high-electron resolution (<0.05 eV) would be required to resolve the Xe 4d ligand field splittings in XeF_2 and XeF_4 and to study the splitting in XeF_6 for the first time. Very recently, we have demonstrated such resolution using monochromatized synchrotron radiation.[42,43]

Using this high instrumental resolution, we report the Xe 4d photoelectron spectra of the three xenon fluorides XeF_x (x = 2, 4, 6) in the gas phase. We had two objectives. First, we wanted to fully resolve and characterize the ligand field splitting in XeF_2 and XeF_4. Second, and by far the most important, we wanted to use the C_2^0 derived from the XeF_6 spectra to estimate to what extent XeF_6 is distorted from octahedral symmetry.

Experimental Section

The samples of XeF_2, XeF_4, and XeF_6 were prepared using previously reported techniques[44-46] and were ascertained to be pure by Raman spectroscopy. The gas-phase Xe 4d spectra of Xe and the XeF_x (x = 2, 4, 6) compounds were recorded at the Canadian Synchrotron Radiation Facility (CSRF) located on the 1 GeV storage ring Aladdin,[47-49] using a high-resolution photoelectron spectrometer.[42,43] The grazing incidence *Grasshopper* monochromator was equipped with a 900 groove/mm holographic grating, which gave a practical minimum photon resolution of 0.15 Å at 25-μm slits. Xe 4d spectra were obtained at 94 eV photon energy using 25 and 50 μm slits, yielding photon resolutions of 0.11 and 0.21 eV, respectively. The photoelectron spectrometer is based on the 36-cm mean radius McPherson electron analyzer, mounted at the pseudomagic angle relative to the polarized synchrotron beam.[42] The electron resolution ($\Delta E/E$ = 1/720) was ~0.035 eV at the ~25 eV kinetic energy used for these spectra.

The volatile samples were leaked into a copper gas cell through a Teflon tube connected directly to the gas cell. Initial spectra showed a prominent band due to Xe gas, which is produced when the xenon fluorides decompose. The samples were allowed to leak into the gas cell until all exposed surfaces were passivated. This passivation process took close to 1 h after which time clean, reproducible Xe 4d spectra of the XeF_x (x = 2, 4, 6) compounds could be readily obtained. At least five high-resolution Xe 4d spectra were obtained for each compound. Our spectrometer gives negligible charging shifts. Therefore the standard deviation of the peak positions and peak widths are generally between 5 and 10 and 5 and 30 meV, respectively (Table I).

The Xe 4d photoelectron spectra were calibrated using the well-characterized Xe $4d_{3/2}$ and $4d_{5/2}$ lines of Xe gas at 69.525 (10) and

(24) Gustev, G. L.; Boldyrev, A. I. *Russ. J. Inorg. Chem.* **1989**, *34*, 598–599.
(25) Bristow, D. J.; Bancroft, G. M. *J. Am. Chem. Soc.* **1983**, *105*, 5634–5638.
(26) Bancroft, G. M.; Creber, D. K.; Basch, H. *J. Chem. Phys.* **1977**, *67*, 4891–4897.
(27) Creber, D. K.; Bancroft, G. M. *Inorg. Chem.* **1980**, *19*, 643–648, and references therein.
(28) Gupta, R. P.; Tse, J. S.; Bancroft, G. M. *Philos. Trans. Roy. Soc.* **1980**, *293*, 535–569.
(29) Bancroft, G. M.; Bristow, D. J.; Tse, J. S. *Chem. Phys.* **1983**, *75*, 277–296.
(30) Bancroft, G. M.; Bristow, D. J. *Can. J. Chem.* **1983**, *61*, 2669–2678.
(31) Edgell, R. G. *Electronic Structure and Magnetism of Inorganic Compounds*; The Royal Society of Chemistry: 1982; Vol. 1, pp 117–120.
(32) Bancroft, G. M.; Tse, J. S. *Comments Inorg. Chem.* **1986**, *5*, 89–118, and references therein.
(33) Ballhausen, C. J. *Introduction to Ligand Field Theory*; McGraw-Hill: New York, 1962.
(34) Jørgensen, C. K. *Modern Aspects of Ligand Field Theory*; North-Holland: Amsterdam, 1971.
(35) Cotton, F. A.; Wilkinson, G. *Advanced Inorganic Chemistry*, 5th ed.; John Wiley and Sons: New York, 1987.
(36) Bancroft, G. M. *Mössbauer Spectroscopy: An Introduction for Inorganic Chemists and Geochemists*; McGraw-Hill: London, 1973.
(37) Sham, T. K.; Bancroft, G. M. *Inorg. Chem.* **1975**, *14*, 2281–2283.
(38) de Waard, H.; Bukshpan, S.; Schrobilgen, G. J.; Holloway, J. H.; Martin, D. *J. Chem. Phys.* **1979**, *70*, 3247–3253, and references therein.
(39) Nielsen, U.; Haensel, R.; Schwarz, W. H. E. *J. Chem. Phys.* **1974**, *61*, 3581–3586.
(40) Comes, F. J.; Haensel, R.; Nielsen, U.; Schwarz, W. H. E. *J. Chem. Phys.* **1973**, *58*, 516–529.
(41) Bancroft, G. M.; Malmquist, P.-Å.; Svensson, S.; Basilier, E.; Gelius, U.; Siegbahn, K. *Inorg. Chem.* **1978**, *17*, 1595–1599.
(42) Bozek, J. D.; Cutler, J. N.; Bancroft, G. M.; Coatsworth, L. L.; Tan, K. H.; Yang, D. S.; Cavell, R. G. *Chem. Phys. Lett.* **1990**, *165*, 1–5.
(43) Bozek, J. D.; Bancroft, G. M.; Cutler, J. N.; Tan, K. H. *Phys. Rev. Lett.* **1990**, *65*, 2757–2760. Bozek, J. D.; Bancroft, G. M.; Tan, K. H. *Phys. Rev. A* **1991**, *43*, 3597–3608.
(44) Syvret, R. G. Ph.D. Thesis, McMaster University, Hamilton, 1987.
(45) Malm, J. G.; Chernick, C. L. *Inorg. Synth.* **1966**, *8*, 254–258.
(46) Chernick, C. L.; Malm, J. G. *Inorg. Synth.* **1966**, *8*, 258–260.
(47) Bancroft, G. M.; Bozek, J. D.; Cutler, J. N.; Tan, K. H. *J. Electron. Spectrosc. Relat. Phenom.* **1988**, *47*, 187–196.
(48) Yates, B. W.; Tan, K. H.; Coatsworth, L. L.; Bancroft, G. M. *Phys. Rev. A* **1985**, *31*, 1529–1534.
(49) Bancroft, G. M.; Bozek, J. D.; Tan, K. H. *Phys. Can.* **1987**, *43*, 113–120.

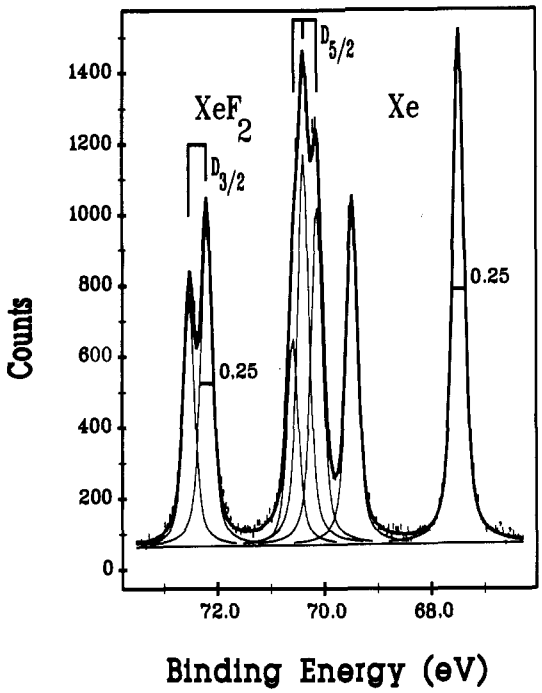

Figure 1. A calibration spectrum of the 4d level in Xe and XeF_2 showing the similar FWHM in both species.

67.541 (9) eV binding energies, respectively.[50] The spectra were fitted using a linear combination of Gaussian and Lorentzian line shapes using an iterative procedure described previously.[51] Except for the three $4d_{5/2}$ peaks of XeF_6, all peak parameters were left unconstrained. In the fitting procedure, the fitted bandwidths at the best photon resolutions gave line widths at half height of close to 0.2 eV with usually ~30% Gaussian and ~70% Lorentzian components. These line shapes reflect the fact that the inherent Lorentzian Xe 4d line width of ≥0.13 eV[42,52] is larger than the total instrumental photon plus electron width (Gaussian) of ~0.11 eV.

Results and Discussion

XeF_2 and XeF_4. A typical Xe 4d calibration spectrum of XeF_2, taken at 94 eV photon energy and an instrumental resolution of 0.21 eV, is shown in Figure 1. Several general features are immediately apparent: (1) the Xe calibrant spectrum consists of two narrow peaks (of 0.25-eV width), due to the spin-orbit splitting in the $4d^9$ ion state; (2) in contrast, the chemically shifted XeF_2 spectrum consists of at least four peaks due to a combination of spin-orbit and ligand field splitting in the ion state; (3) the XeF_2 line widths are within 0.01 eV of the Xe linewidths, showing that vibrational broadening is very small indeed in XeF_2, as previously assumed;[41] and (4) the line widths in even this "medium"-resolution spectrum are much narrower than in the previous best photoelectron spectrum (see, for example, Figure 3 in ref 41); and are as good as, or better than, the previously published photoabsorption spectrum.[40] The chemical shift for XeF_2 of ~2.8 eV is in excellent agreement with values from the previous low-resolution spectra.[8,41,53] Obviously, the increased resolution has dramatically increased the chemical shift sensitivity of the photoelectron technique.

Higher resolution photoelectron spectra (at 0.11 eV instrumental resolution) of XeF_2 and XeF_4 are shown in Figure 2. For XeF_2, the five peaks are now more apparent than in Figure 1. The small peak at 69.53 eV is due to the Xe $4d_{3/2}$ peak of Xe gas. The XeF_4 spectrum is qualitatively similar to the XeF_2 spectrum. The two weak peaks at low binding energy in the XeF_4 spectrum are due to the $4d_{3/2}$ peaks of the decomposition product XeF_2. Table I summarizes the peak positions, widths, and standard deviations for peaks 1–5 in the two spectra. Looking more carefully at Figure 2 and Table I, significant differences between the XeF_2 and XeF_4 spectra become apparent. First, the $4d_{5/2}$ splitting pattern in the two spectra is quite different: in XeF_2, peak 5 is well-separated and resolved, whereas in XeF_4, peak 3 is well-resolved. As seen below, this is due to the different sign of C_2^0 because of the different structures. Second, while the line widths of XeF_2 of <0.24 eV

Table I. Photoelectron Experimental Data for Xe, XeF_2, XeF_4, and XeF_6 (eV)[c]

compd		peak position (eV)	peak width (eV)
Xe	1	69.525 (10)	0.207 (4)
	2	67.541 (9)	0.202 (4)
XeF_2	1	72.568 (6)	0.248 (8)
	2	72.248 (6)	0.223 (10)
	3	70.601 (13)	0.264 (26)
	4	70.421 (9)	0.256 (27)
	5	70.179 (6)	0.214 (19)
XeF_4	1	75.098 (6)	0.319 (8)
	2	74.729 (7)	0.255 (8)
	3	73.140 (10)	0.392 (10)
	4	72.816 (10)	0.210 (27)
	5	72.661 (5)	0.225 (26)
XeF_6[a]	1	77.450 (13)	0.35 (4)
	2	77.317 (11)	0.30 (3)
	3	75.51	0.34
	4	75.37	0.28
	5	75.24	0.28
XeF_6[b]	1	77.462 (13)	0.32 (4)
	2	77.321 (11)	0.25 (3)
	3	75.53	0.33
	4	75.38	0.25
	5	75.25	0.25

[a,b] *a* and *b* refer to Figures 4a and 4b, respectively, which were taken at experimental resolutions of 0.21 and 0.11 eV, respectively. [c]The values in the brackets are the standard deviations of the positions and widths.

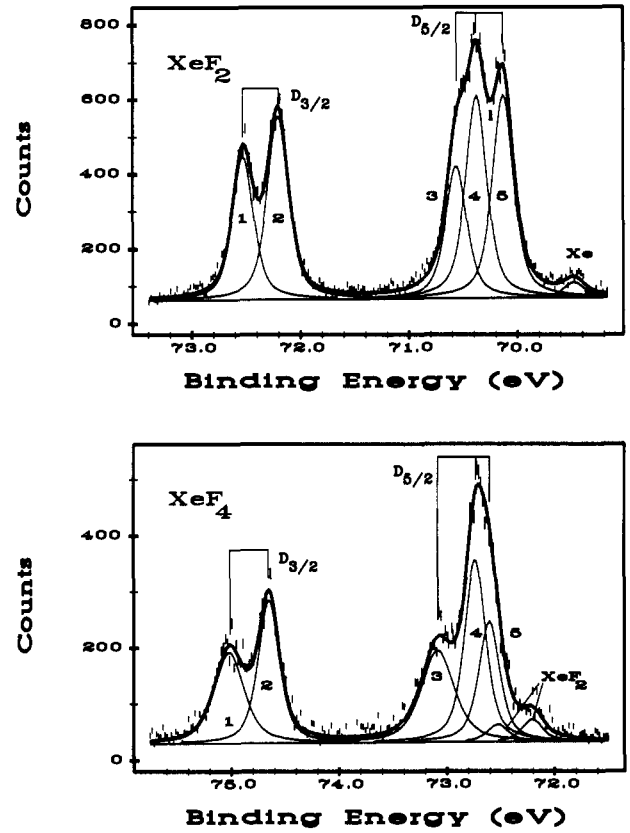

Figure 2. The ligand field splitting in XeF_2 and XeF_4. These spectra show the resolved splitting patterns. The thin lines are a best fit to the spectra.

(50) Krause, M. O. *Synchrotron Radiation Research*; Winick, H., Doniach, S., Eds.; Plenum Press: New York, 1980; pp 101–158.
(51) Bancroft, G. M.; Adams, I.; Coatsworth, L. L.; Bennewitz, C. D.; Brown, J. D.; Westwood, W. D. *Anal. Chem.* **1975**, *47*, 586–588.
(52) King, G. C.; Tronc, M.; Read, F. H.; Bradford, R. C. *J. Phys. B* **1977**, *10*, 2479–2495.
(53) Siegbahn, K. et al. *ESCA Applied to Free Molecules*; North-Holland Publishing Co.: New York, 1971; pp 132–136.

Table II. Ligand Field and Spin-Orbit Splitting Parameters for XeF_2, XeF_4 and XeF_6 (eV)[b]

	XeF_2		XeF_4		
	this work	Bancroft et al.[41]	this work	Bancroft et al.[41]	XeF_6
C_2^0	+0.0391 (2)	+0.041 (4)	−0.0468 (10)	−0.045 (4)	−0.018 (2) −0.008[a]
C_4^0	+0.0010 (2)		−0.0003 (10)		
λ	0.814 (3)		0.822 (3)		0.807 (4)
$5/2\lambda$	2.035 (3)	1.98 (2)	2.055 (3)	2.00 (1)	2.018 (4)
E_{4d}	71.212 (3)	71.13 (2)	73.679 (3)	73.60 (1)	76.118 (4)
ΔE_{4d}	2.877 (3)	2.84 (1)	5.344 (3)	5.30 (1)	7.783 (4)
ΔE_{3d}[8]		2.87		5.41	7.64

[a] Values for solid-state XeF_6 are predictions based on quadrupole splittings obtained from Mössbauer data. See body of text. [b] The values in the brackets are the standard deviations.

are within 0.04 eV of Xe gas, the XeF_4 line widths—especially peaks 1 and 3—are significantly broader. Undoubtedly, some of this broadening is vibrational or chemical in origin (see below).

The five observed peaks of XeF_2 and XeF_4 in Figure 2 are due to a combination of spin-orbit and ligand field effects which remove the degeneracy of the d^9 final state. The Hamiltonian for the d^9 hole state in $D_{\infty h}$ (XeF_2), D_{4h} (XeF_4), and C_{3v} (XeF_6) symmetries simplifies to eq 1.[33,34] Diagonalizing the Hamiltonian in d electron

$$H = H_0 + C_2^0[3L_z^2 - L(L+1)] + C_4^0[35L_z^4 - 30L(L+1)L_z^2 + 25L_z^2 - 6L(L+1) + 3L^2(L+1)^2] + \lambda\,[\tfrac{1}{2}(L_+S_- + L_-S_+) + L_zS_z] \quad (1)$$

subspace and treating d^9 and d^1 with the usual sign changes, the eigenvalues and eigenfunctions can be calculated[26,32,33] (Tables II and III).

The five equations derived from eq 1 comprise a nonlinear overdetermined system thereby making exact solutions for E_{4d}, C_2^0, C_4^0, and λ impossible. It was decided that two different techniques should be used to calculate the ligand field parameters reported in Table II. A nonlinear least-squares fitting procedure and a Monte Carlo simulation were both applied to the five equations so that a global minimum could be obtained. The values calculated by the two techniques are in excellent agreement and the average is reported in Table II.

The parameters (Table II) are in remarkably good agreement with those obtained earlier in the lower resolution study;[41] but the errors (standard deviations from ten separate spectra) on C_2^0 are much smaller in our present study. C_4^0 is insignificant for both compounds. The calculated peak positions using the best-fit parameters in Table II are in excellent agreement with the experimental peak positions (Table III). Indeed, in XeF_2 and XeF_4, the calculated and experimental positions agree to within 0.03 eV. The eigenfunctions in Table III are also in remarkably good agreement with those derived from the previous photoabsorption study,[40] especially considering that only two of the five peaks were resolved in XeF_4.[40]

The spin-orbit splittings are slightly larger than the splittings for atomic Xe of 1.984 eV (Table I). We believe that this increase is real. However, if the splitting is fixed at 1.984 eV in XeF_2 and XeF_4, the C_2^0 values do not differ significantly from those in Table II.

As indicated above by the different splitting pattern for the $D_{5/2}$ level in XeF_2 and XeF_4, the signs of C_2^0 are opposite in the two compounds. The positive and negative signs for C_2^0 in linear XeF_2 and square-planar XeF_4 are expected and reflected in the wave functions in Table III. The positive C_2^0 (and positive eq_n) in XeF_2 arises because the electronegative F ligands withdraw $5p_z$ electron density from the Xe atom thereby making $n_{p_z} < {}^1/_2(n_{p_x} + n_{p_y})$. There is a depletion of valence p electron density along the molecular z-axis. In XeF_4, the opposite is true, and there will obviously be a surplus of valence p electron density along the molecular z-axis. In an octahedral molecule such as XeF_6, no splitting would be expected. Precisely these arguments are used in rationalizing positive and negative eq_n values.[36,54]

Table III. One-Electron Eigenfunctions and Eigenvalues for the Xe 4d levels in XeF_2 and XeF_4[a]

	M_j	term	eigenfunction	energy (eV) expt	energy (eV) calcd
XeF_2	1/2	$\Pi_{1/2}$	$0.74\|1\beta\rangle - 0.68\|0\alpha\rangle$	72.568	72.597
	3/2	$\Delta_{3/2}$	$0.86\|2\beta\rangle - 0.50\|1\alpha\rangle$	72.248	72.276
	1/2	$\Sigma_{1/2}$	$0.68\|1\beta\rangle + 0.74\|0\alpha\rangle$	70.601	70.602
	3/2	$\Pi_{3/2}$	$0.50\|2\beta\rangle + 0.86\|1\alpha\rangle$	70.421	70.402
	5/2	$\Delta_{5/2}$	$\|2\alpha\rangle$	70.179	70.175
XeF_4	3/2	$e_{g3/2}'$	$0.92\|2\beta\rangle - 0.38\|1\alpha\rangle$	75.098	75.120
	1/2	$e_{g1/2}'$	$0.80\|1\beta\rangle - 0.60\|0\alpha\rangle$	74.729	74.719
	5/2	$e_{g5/2}''$	$\|2\alpha\rangle$	73.140	73.134
	3/2	$e_{g3/2}''$	$0.38\|2\beta\rangle + 0.92\|1\alpha\rangle$	72.816	72.800
	1/2	$e_{g1/2}''$	$0.60\|1\beta\rangle + 0.80\|0\alpha\rangle$	72.661	72.624

[a] $|0\rangle$, $|1\rangle$, and $|2\rangle$ refer to (d_{z^2}), (d_{xz}, d_{yz}) and $(d_{xy}, d_{x^2-y^2})$, respectively.

The ordering of the d orbitals indicated by the wave functions in Table III can be rationalized by simple electrostatic arguments. Because there is a depletion of p_z valence electron density in XeF_2, the z-type 4d orbitals in XeF_2 will be *stabilized*, and the energy ordering is $d_{z^2} < d_{xz},d_{yz} < d_{xy},d_{x^2-y^2}$ ($|0\rangle < |1\rangle < |2\rangle$), resulting in the opposite ordering of binding energies, $|0\rangle > |1\rangle > |2\rangle$, for XeF_4 as is apparent from Table III, e.g., the order of binding energies is $\Sigma_{1/2}$ (majority $|0\rangle$) > $\Pi_{3/2}$ (majority $|1\rangle$) > $\Delta_{5/2}$ (majority $|2\rangle$).

When Table I is examined, it is immediately apparent that a line broadening is observed going from Xe gas to XeF_2 and XeF_4. There are two possible mechanisms to account for this behavior. The first is due to a vibrational broadening of the lines from $\nu = 0 \rightarrow \nu' = 0, 1, 2...$ etc. transitons in the ion state. Previous work on the Zn 3d and Cd 4d levels[26-32] shows that substantial vibrational effects are not generally important on d-levels. More importantly, our unpublished Ge 3d spectrum of GeH_4 (to be published) shows no hint of vibrational effects; in great contrast to the extensive vibrational effects in the Si 2p levels of SiH_4.[42,43] The second mechanism involves a chemical effect on the line widths due to a change in Auger decay rates from a loss of Xe valence electron density in the xenon fluorides relative to atomic Xe. Recent experimental and theoretical work on C 1s levels[55] shows that this chemical effect can be important in changing core level line widths, and our recent work on the I 4d levels in I compounds shows that this effect is much more important than vibrational broadening in I compounds[58] and probably in our Xe compounds. We are observing predominantly $\nu = 0 \rightarrow \nu' = 0$ transitions for all peaks, as is strongly shown by the good agreement between observed and calculated energies in Table III.

The wave functions in Table III are important in rationalizing the first broadening mechanism (Table I). For example, in XeF_2 none of the 4d lines are broadened greatly relative to the Xe gas 4d lines; but peak 1, which corresponds to the orbital with high

(54) Bancroft, G. M.; Platt, R. H. *Adv. Inorg. Radiochem.* **1972**, *15*, 59–258.

(55) Coville, M.; Thomas, T. D. *Phys. Rev. A* **1991**, *43*, 6053–6056, and references therein.

(56) Tsao, P.; Cobb, C. C.; Claassen, H. H. *J. Chem. Phys.* **1971**, *54*, 5247–5253.

(57) McGuire, E. J. *Phys. Rev. A* **1974**, *9*, 1840–1851.

(58) Cutler, J. N.; Bancroft, G. M.; Sutherland, D. G.; Tan, K. H. *Phys. Rev. Lett.* **1991**, *67*, 1531–1534.

d_{z^2} character pointed toward the F ligands, is broader than peak 2, which corresponds to d orbitals not pointing toward the F ligands. The symmetric stretching frequency, ν_1, for XeF_2 is only 514.5 cm^{-1} (64 meV).[56] The lack of appreciable broadening or asymmetry of the lines shows that any vibrational broadening is very small with $\nu = 0 \rightarrow \nu' = 0$ being by far the predominant transition, with perhaps a small $\nu = 0 \rightarrow \nu' = 1$ contribution to peak 1.

In XeF_4 considerable broadening is observed in peaks 1 and 3 (Table I). Some vibrational broadening (ν_1 = 554.3 cm^{-1}, 69 mev)[56] would be expected on the orbitals with d character in the x–y plane (corresponding to peaks 1 and 3) and directed toward the F ligands. The other d orbitals directed away from the F ligands have a FWHM similar to XeF_2 indicating little or no vibrational broadening.

In the second mechanism, the change of electron density in the Xe 5p orbitals changes the rate of Auger decay into the core hole and is reflected by the line width increase. McGuire[57] calculated that the lifetime of the Xe $N_{4,5}$ shells should be substantially narrower (~80 meV) than the surrounding $N_{4,5}$ shells (Sn: ~140 meV). Also, our measured I 4d line widths[58] of 0.2–0.3 eV are much broader than the atomic Xe 4d line widths of ~0.13 eV.[42,52] The increase in line width from Xe to XeF_x (x = 2, 4, 6) is in excellent agreement with the multicenter model used by Hartmann,[59] but opposite to the one center model of Thames and Coville. The former model predicts an increase in the line width for the C 1s core level when the electronegativity of the ligand is increased. (This is the opposite trend to that observed and predicted for C 1s and I 4d line widths[55,58].) When one examines the line widths of the peaks with a majority of orbital character perpendicular to the Xe–F bond, the line widths increase from 0.202 eV for Xe, to 0.223 eV for XeF_2, and 0.255 eV for XeF_4 as the amount of 5p density withdrawn from the Xe atom increases. These increased line widths approach I 4d inherent line widths of 0.20 to 0.25 eV for ICl and IBr.[58] Some of the broadening of the peaks 1 and 3 in XeF_2 and XeF_4 will also be due to this chemical effect.

XeF_6. High-resolution Xe 4d spectra of Xe gas and XeF_6 are shown in Figure 3. A hint of the $4d_{3/2}$ peaks of XeF_4, from decomposition, are also seen at ~75 eV binding energy. Although no ligand field splitting is resolved in the XeF_6 spectrum, the XeF_6 lines are about double the line width of Xe lines (0.36 and 0.40 eV versus 0.20 eV). We attribute this large broadening of the XeF_6 peaks to unresolved ligand field splitting from a distorted C_{3v} XeF_6 structure.

Before fitting this spectrum to the characteristic five peaks, it is important to comment on three other line broadening mechanisms—vibrational broadening, chemical shift broadening due to two (or more) XeF_6 structures (e.g., C_{3v} and C_{2v}) which are "frozen out" by the fast photoelectron technique, and the above chemical effect on the Auger rates due to a decrease in Xe 5p electron density. Vibrational broadening cannot be the major broadening mechanism for three reasons. First, the symmetric ground-state vibrational frequency of XeF_6 (ν_1 = 608 cm^{-1}, 75 meV)[18] is comparable to those for XeF_2 and XeF_4. Very large vibrational broadening would not be expected for XeF_6 because substantial vibrational broadening was not observed at all for XeF_2 and only on the two peaks of high $d_{x^2-y^2}$ and d_{xy} character in XeF_4 (Table I). Second, and more significant, vibrational broadening would result in the same $4d_{3/2}$ and $4d_{5/2}$ widths, whereas the widths of 0.36 and 0.40 eV are substantially different. Two (or more) different structures can also be ruled out as controlling the broadening mechanism. Like vibrational broadening, several structures would lead to the same widths for both 4d lines. In addition, Bristow and Bancroft[25] showed that the observed vibrational features observed on the $8a_{1g}$ valence band orbital could be explained by a single gas-phase structure. Also, the recent analysis of the broad F1s spectrum[24] of XeF_6 gives reasonable evidence for the two nonequivalent fluorines in one C_{3v} structure. Thirdly, a line broadening due to the chemical effect is an unlikely

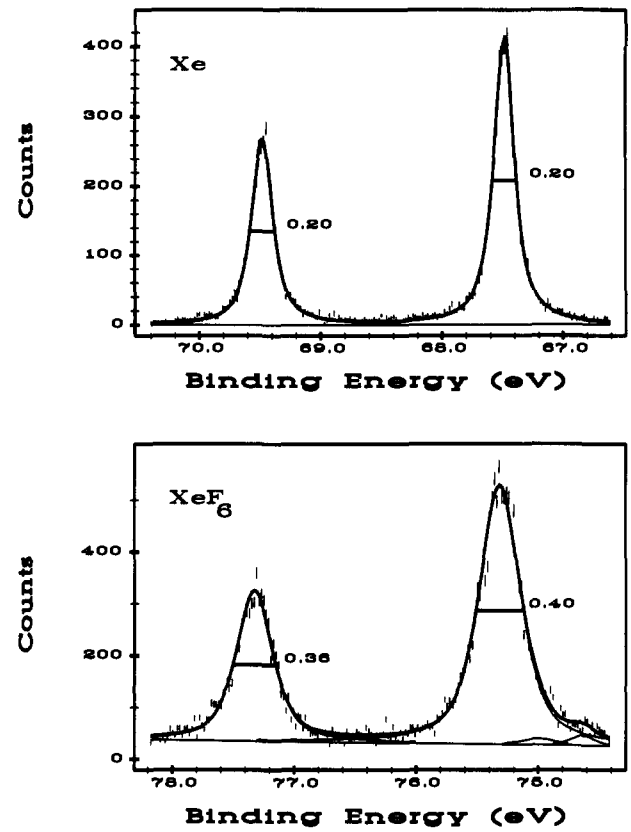

Figure 3. A comparison of the 4d region of Xe and XeF_6. It is apparent that XeF_6 has substantially broader lines than in Xe. This broadening is due to ligand field splitting of the core 4d level.

mechanism to account for the substantial increase in line widths. As was observed in XeF_2 and XeF_4, three of the line widths increased by only ~20 and ~50 meV, respectively. An increase in line width of 160 meV due to a loss of Xe 5p electron density seems very unlikely. If one assumes a linear relationship between line widths and electron density, a line broadening of only ~70–80 meV would be expected for XeF_6. This value is one-half of the measured line broadening which indicates that a chemical effect is only a small component of the observed line broadening.

Unresolved ligand field splitting is the only mechanism that would yield such broad *and* different Xe $4d_{3/2}$ and $4d_{5/2}$ widths. Figure 4 shows the five peak fits to two spectra (of over 10) taken at the two different photon resolutions. The $4d_{3/2}$ doublet was fit *without* any constraints. The two peak positions and widths (peaks 1 and 2, Table I) are in excellent agreement, and the standard deviation from other spectra at each resolution are small (~10 meV). The $4d_{3/2}$ splitting of 0.15 eV (which is used below to obtain C_2^0) is certainly accurate to ±0.02 eV. The three peak fit to the $4d_{5/2}$ triplet is not unique, so we do not use these positions to calculate C_2^0. However, reasonable line width and line shape constraints from the XeF_2 and XeF_4 fits give good reproducibility for the three peak positions (Table I).

The derived chemical shift, ligand field, and spin-orbit parameters for XeF_6 are given in Table II. The chemical shift is very large and in agreement with previous measurement from the Xe 3d levels.[8] The C_2^0 value of 0.018 ± 0.002 eV, derived from the $4d_{3/2}$ splitting using the following formula[28]

$$\frac{\Delta E_{3/2XeF_6}}{\Delta E_{3/2XeF_2}} = \frac{C^0_{2XeF_6}}{C^0_{2XeF_2}} \qquad (2)$$

is less than one-half of those for XeF_2 and XeF_4. Equation 2 is a good approximation when the spin-orbit splitting is large compared to C_2^0 as shown from $d_{3/2}$ splittings of XeF_2 and XeF_4. A C_2^0 for XeF_4 of −45.2 meV, determined from the $d_{3/2}$ splittings of XeF_2 and XeF_4 and the C_2^0 of XeF_2, is in good agreement with the experimentally determined value of −46.8 meV. The sign of

(59) Hartmann, E. *J. Phys. B* **1988**, *21*, 1173–1182.

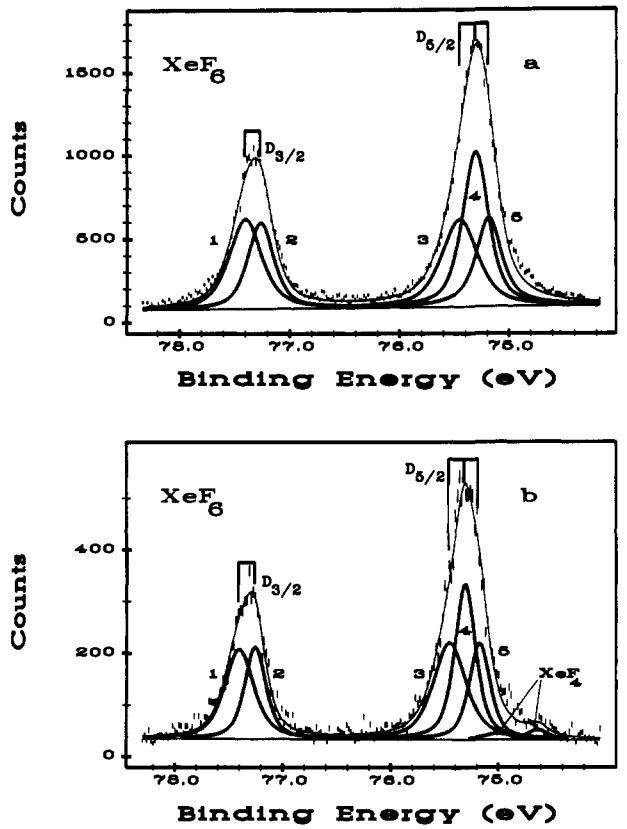

Figure 4. The best five peak fits to the gas-phase 4d spectrum of XeF_6 taken at two different resolutions: (a) at 50 μm (ΔE = 0.21 eV) and (b) at 25 μm (ΔE = 0.11 eV). The five peak fit of spectra (b) are statistically better than the single band fit in Figure 3.

C_2^0 cannot be obtained directly from the spectrum, but we assign a negative sign based on what structure is reasonable (see below).

Qualitatively, the C_2^0 value of −0.018 ± 0.002 eV shows immediately that XeF_6 is distorted considerably from octahedral symmetry. To obtain F–Xe–F bond angles, we can use an adaptation of the additive partial quadrupole splitting (PQS) treatment,[54,60] used to obtain bond angles and structure in Sn compounds[36,37] and solid-state XeF_6.[38] For ^{129}Xe quadrupole splittings (ΔE_Q) for the xenon fluorides, we can write[34,54,60]

$$\Delta E_Q = (PQS)_F \sum_F (3\cos^2\theta - 1) \quad (3)$$

Because the quadrupole and C_2^0 Hamiltonians transform identically, we can write by analogy

$$C_2^0 = (PLFS)_F \sum_F (3\cos^2\theta - 1) \quad (4)$$

where PLFS is the partial ligand field splitting for F in the xenon fluorides, and θ is the angle between the molecular z-axis and the bond of interest. Before using this model for the first time for ligand-field splittings, it is important to review the assumptions involved and the expected validity and accuracy of the model.[60] First, we assume that C_2^0, like e^2qQ, can be regarded as the sum of *independent* contributions, one from each F bound to Xe. Second, we assume that the PLFS for F is *constant* in all Xe–F compounds. This implies that each F withdraws the same amount of Xe 5p valence electron density (or the Xe–F bond character is constant), and the Xe–F bond lengths are consistent in all compounds containing Xe–F bonds. Third, we assume any relaxation contributions to C_2^0 are negligible or constant in all Xe–F compounds. Fourth, we assume that the principal ligand field axis corresponds to the molecular symmetry axis in all compounds.

The first two assumptions could be challenged immediately by the rather large difference in Xe–F bond lengths in two-, four-, and six-coordinate Xe compounds[38] (see Table IV). However,

(60) Bancroft, G. M. *Coord. Chem. Rev.* **1973**, *11*, 247–262.

Table IV. Bond Lengths and ^{129}Xe Quadrupole Splittings of Selected Xenon Compounds in the 2+, 4+, and 6+ Oxidation States

compd	Xe–F bridging (Å)	Xe–F terminal (Å)	ΔE_Q (mm s^{-1})	ref
XeF_2		2 × 2.00	39.7 (4)	2
$XeF_2 \cdot 2WOF_4$	2.04	1.89	41.0 (3)	38
$XeF^+Sb_2F_{11}^-$	2.35	1.84	41.5 (2)	38
$Xe_2F_3^+AsF_6^-$	2.14	2 × 1.90	41.3 (2)	38
XeF_4		4 × 1.953	41.04 (7)	38
$XeF_3^+BiF_6^-$	2.25	1.81, 2 × 1.93	41.3 (1)	38
XeF_6(tetramer)	2.23/2.60 (3)	1.86 (3), 1.84 (3)	7.7 (2)	13
XeF_6 (hexamer)	2.56 (2)	1.76 (3), 1.96 (2)		

there is still considerable evidence that the model can be used quantitatively. Thomas pointed out[8] that the Xe 3d and Xe 4d photoelectron chemical shifts show that each F in XeF_2, XeF_4, and XeF_6 have the same charge and indeed withdraws the same amount of Xe valence electron density. Perhaps more relevant to the additive model, the ^{129}Xe quadrupole splittings (ΔE_Q) for a large number of compounds are within ±4% of that predicted from the additive model regardless of bond lengths. For example, the $|E_Q|$ values for linear XeF_2 and $XeF^+Sb_2F_{11}^-$ [θ = 0°, ΔE_Q = 4$(PQS)_F$] are 39.7 and 41.5 mm s^{-1}, respectively, while the $|\Delta E_Q|$ values for square-planar XeF_4 and $XeF_3^+BiF_6^-$ [θ = 90°, ΔE_Q = −4$(PQS)_F$] are 41.0 and 41.3 mm s^{-1}, respectively. The additive model above indicates that the ΔE_Q values for XeF_2 should be equal to the ΔE_Q for XeF_4, but the signs should be opposite. The sign of ^{129}Xe ΔE_Q cannot be measured readily, whereas the signs of C_2^0 can be measured directly, but the $|\Delta E_Q|$ values for XeF_2 and XeF_4 are again within 5% of each other. The above values show that ΔE_Q is not sensitive to the individual bond lengths or bond characters as assumed in the model. In addition, the ΔE_Q value for the distorted XeF_6 octahedron in the solid state (7.7 mm s^{-1} [38]) is rationalized very well by the additive model, demonstrating the strong dependence of ΔE_Q on the distortion of the octahedron. The ^{119}Sn and ^{57}Fe ΔE_Q values[37,54,60] also demonstrate that ΔE_Q is not sensitive to small changes in metal ligand character but is very sensitive to bond angle changes.[37]

The above evidence strongly indicates that we can use eq 4 to obtain bond angles in XeF_6. We first derive the $(PLFS)_F$ value from the C_2^0 values for XeF_2 and XeF_4. The value for $(PLFS)_F$ from the two compounds are +0.0098 and +0.0117 eV, respectively. Using the average of these two values (+0.0108 eV) and assuming the C_{3v} structure (Figure 5) for XeF_6, we can write

$$C_2^0 = 3(PLFS)_F(3\cos^2\theta_{1,2,3} - 1) + 3(PLFS)_F(3\cos^2\theta_{4,5,6} - 1) \quad (5)$$

It was not possible to solve $\theta_{1,2,3}$ and $\theta_{4,5,6}$ concurrently. Therefore to solve eq 5, the angle $\theta_{1,2,3}$ was held constant at different fixed angles (48°, 50°, 52°, and 54.7°) and $\theta_{4,5,6}$ was allowed to float. Figure 5 is a plot of C_2^0 versus $\theta_{4,5,6}$ while holding $\theta_{1,2,3}$ constant. From the electron diffraction[16,17] and latest theoretical values[21] for $\theta_{1,2,3}$ of 49° and 52° respectively, we fix $\theta_{1,2,3}$ at 50°. The two boxed-in regions refer to the experimentally measured C_2^0 and the size of the boxes gives the estimated error, which we take as 50% greater than the standard deviation in C_2^0, due to deficiencies in the model.

Since it is not possible to directly determine the sign of C_2^0 for XeF_6, two possible angles for $\theta_{4,5,6}$ are possible. If C_2^0 is positive, the F–Xe–F angle falls between 77 and 84° indicating that the angle defined by $\theta_{4,5,6}$ is closing up and the lone pair of electrons are acting like a ring of charge in the x–y plane forcing the ring to close. In the negative C_2^0 case, the F–Xe–F angle is 111–117° thereby forcing $\theta_{4,5,6}$ to open up, indicating that the lone pair is directed toward the face of the cone.

The majority of the experimental and latest theoretical results suggest strongly that the latter distortion takes place, and thus C_2^0 is negative. This gives estimates for $\theta_{1,2,3}$ and $\theta_{4,5,6}$ of 50 ± 2° and 76 ± 4°, respectively. These angles are in good agreement with the latest theoretical values of 49° and 76°, respectively,[21] but not in as good agreement with the electron diffraction results of 52° and 67°, respectively.[16,17]

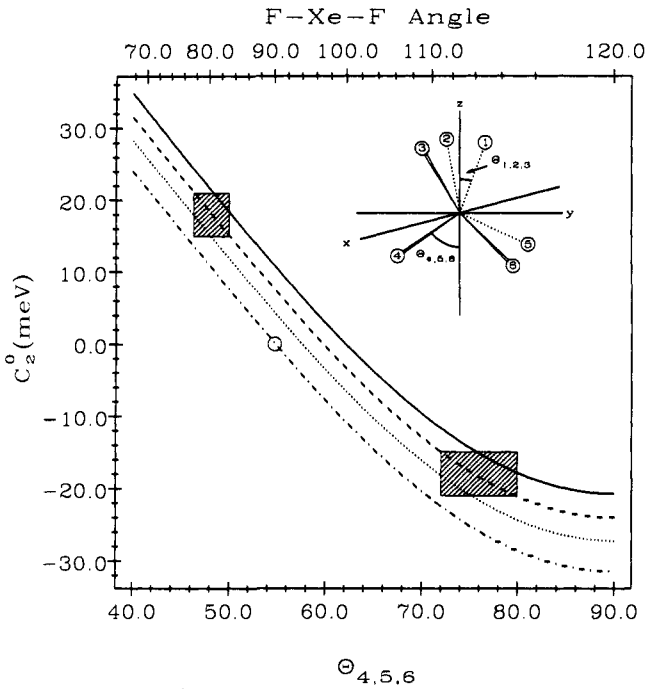

Figure 5. Plot of C_2^0 versus $\Theta_{4,5,6}$ (and F-Xe-F bond angle) for different $\Theta_{1,2,3}$ values (48° —, 50° – –, 52° ···, 54.7° –·–). (O) represents the position of XeF_6 if it is perfectly octahedral. (The F-Xe-F angles are 90° and Θ_{1-6} is 54.7°.) In the case of $\Theta_{1,2,3}$ being 50°, the errors on C_2^0 and $\Theta_{4,5,6}$ are given by the dimensions of the box.

Finally, it is interesting to note that our C_2^0 value is much larger than that expected from the known solid-state structure.[13] A C_2^0 value for the solid-state structure (-0.008 eV in Table II) can be estimated readily using the Mössbauer e^2qQ values in the solid state[38,61] and using the known proportionality of C_2^0 and e^2qQ:[28]

$$\frac{(e^2qQ)_{XeF_6}}{(e^2qQ)_{XeF_2}} = \frac{(C_2^0)_{XeF_6}}{(C_2^0)_{XeF_2}} \quad (6)$$

Using the e^2qQ values for XeF_2 and XeF_6 of +39.7 and ±7.7 mm s^{-1}, and the C_2^0 value of XeF_2, the C_2^0 value of ±0.008 eV can be readily calculated. This smaller C_2^0 value for the solid-state structure is consistent with the smaller (and different) distortion of XeF_6 in the solid state.

Conclusions

We have resolved ligand field splittings by photoelectron spectroscopy in relatively deep core levels ($E_B > 30$ eV) for the first time. To resolve these effects, it required very high resolution not previously attained in the gas phase. The spectra have been characterized using a simple Hamiltonian involving crystal field splitting and spin-orbit splitting.

Of particular interest, we have estimated the gas-phase structure of XeF_6 from the Xe 4d spectra using an additive model similar to that used in Mössbauer spectroscopy. It has been shown that for a C_{3v} XeF_6 structure, $\Theta_{1,2,3} = 50°$ and $\Theta_{4,5,6} = 76 \pm 4°$. This is perhaps the best experimental evidence of the distortion of gas-phase XeF_6, and it is shown to be in excellent agreement with the recent calculations of Klobukowski et al.[21]

Acknowledgment. The authors thank Dr. John Tse for many helpful and thought provoking discussions and the staff at the Synchrotron Radiation Center (Stoughton) for their technical support. We are grateful to the National Research Council (NRC) of Canada, the Natural Sciences and Engineering Research Council (NSERC) of Canada, and to the U.S. Air Force Astronautics Laboratory, Edwards AFB, California (GJS) for financial support.

Registry No. XeF_2, 13709-36-9; XeF_4, 13709-61-0; XeF_6, 13693-09-9; Xe, 7440-63-3; F_2, 7782-41-4.

(61) Perlow, G. J.; Perlow, M. R. *J. Chem. Phys.* **1968**, *48*, 955-961.

An Unusual Relationship between the N-F Bond Lengths and Force Constants in *N*-Fluoroamines

Dines Christen,[1a] Om Dutt Gupta,[1b] Johannes Kadel,[1a] Robert L. Kirchmeier,[1b] Hans Georg Mack,[1a] Heinz Oberhammer,*[1a] and Jean'ne M. Shreeve[1b]

Contribution from the Institut für Physikalische und Theoretische Chemie, Universität Tübingen, 7400 Tübingen, Germany, and the Department of Chemistry, University of Idaho, Moscow, 83843 Idaho. *Received May 20, 1991*

Abstract: The gas-phase structure of fluorodimethylamine, Me_2NF, has been studied by electron diffraction and microwave spectroscopy. A joint analysis of diffraction intensities and rotational constants results in the following skeletal geometric parameters (r_z values with 3σ uncertainties): N-F = 1.447 (6) Å, N-C = 1.462 (7) Å, ∠CNC = 112.0 (10)°, and ∠FCN = 103.6 (5)°. The N-F bond lengths in the series Me_nNF_{3-n} increase strongly from 1.371 (2) Å in NF_3 to 1.447 (6) Å in Me_2NF. Attempts to derive clear-cut N-F force constants for the fluoromethylamines $MeNF_2$ and Me_2NF from vibrational frequencies failed. Ab initio calculations at the MP2/6-31G** level reproduce the experimental N-F bond lengths and the vibrational frequencies of this series very well. The calculated N-F force constants *increase* with *increasing* bond lengths from 4.58 mdyn $Å^{-1}$ in NF_3 to 4.77 mdyn $Å^{-1}$ in Me_2NF. An explanation of this unusual bond length-force constant relationship on the basis of polar effects is proposed.

Introduction

There exists no obvious a priori reason for any correlation between the length and the force constant of a certain bond. The length is determined by the position and the force constant by the curvature of the potential minimum. Nevertheless, an inverse relation between these two quantities is widely assumed and several empirical expressions have been proposed on the basis of experimental data. Badger[2] suggested the relation $f = [a(r - b)]^{-1/3}$

(1) (a) Tübingen. (b) Idaho.

(2) Badger, R. M. *J. Chem. Phys.* **1934**, *2*, 128; **1935**, *3*, 710.

0002-7863/91/1513-9131$02.50/0